

Structural and magnetic study of $\text{PrBaCo}_2\text{O}_{5+\delta}$ ($\delta \approx 0.75$) cobaltite

Carlos Frontera, José Luis García-Muñoz, and Anna E. Carrillo

Institut de Ciència de Materials de Barcelona, CSIC, Campus Universitari de Bellaterra, E-08193 Bellaterra, Spain

Clemens Ritter

Institut Laue Langevin, 6, rue Jules Horowitz, F-38042 Grenoble Cedex 9, France

David Martín y Marero

*Institut Laue Langevin, 6, rue Jules Horowitz, F-38042 Grenoble Cedex 9, France,
and Instituto de Ciencia de Materiales de Aragón, CSIC, Zaragoza, Spain*

Alberto Caneiro

Centro Atómico de Bariloche, 8400-San Carlos de Bariloche, Argentina

(Received 10 June 2004; revised manuscript received 22 September 2004; published 23 November 2004)

We have investigated the structural and magnetic properties of $\text{PrBaCo}_2\text{O}_{5+\delta}$ ($\delta \approx 0.75$) layered cobaltite. By means of neutron and synchrotron x-ray powder diffraction we have determined the ordered distribution of oxygen vacancies in PrO_δ planes. This order doubles both a and b lattice parameters from the perovskite cell parameter, forming a tetragonal (rather than orthorhombic) structure. On cooling, a paramagnetic to ferromagnetic and an incomplete ferromagnetic to antiferromagnetic transition take place. This second transition leads to a coexistence of ferromagnetic and antiferromagnetic order, forming a canted G -type antiferromagnetic structure. Magnetic data above the ferromagnetic transition evidence a large value of the effective paramagnetic moment of Co, implying that, well below room temperature, Co^{3+} ions in an octahedral environment present a high-spin state, in contrast to $\text{RBaCo}_2\text{O}_{5.5}$ cobaltites.

DOI: 10.1103/PhysRevB.70.184428

PACS number(s): 75.25.+z, 71.27.+a, 75.80.+q

I. INTRODUCTION

The study of transition-metal oxides is, nowadays, very extended in the field of materials science. Among them, cobalt oxides are the subject of vivid studies. In cobaltites the spin state degree of freedom of Co ions introduces new interesting effects in the case of narrow-band oxides. Among other families like misfit cobaltites for thermopower applications^{1,2} or mixed-valence cobalt perovskites as candidates to present charge ordering like $\text{Pr}_{0.5}\text{Ca}_{0.5}\text{CoO}_3$,³ layered cobaltites with general formula $\text{RBaCo}_2\text{O}_{5+\delta}$ ($R \equiv$ rare earth, $0 \leq \delta \leq 1$) have been the subject of several studies during the last years.⁴⁻¹⁵ These compounds have been demonstrated to be complex systems presenting very intriguing phenomena like charge ordering,^{4,5} metal-insulator transitions,^{6,7} orbital order,⁸ and also a large thermoelectric power.¹² Following the paper by Troyanchuk *et al.*,⁶ the cornerstone paper by Maignan *et al.*⁷ evidenced that the oxygen content of these compounds can be tailored by heat treatments in different atmospheres. Maignan *et al.*⁷ also established two special structural features: the ordering in alternating planes of Ba and R ions and the tendency of oxygen vacancies to place at the R planes forming ordered patterns.

The most appealing features of narrow-band cobaltites are the spin-charge-orbital coupling and the fact that Co presents, with great facility, transitions between different spin states. As an example one can mention the case of LaCoO_3 , object of great controversy during the 1980s and 1990s (Ref. 16). The competition between the Hund exchange and the crystal field, together with the distortions in octahedral coordination or the presence of pyramidal coordination, can sta-

bilize three different spin states: low spin (LS), intermediate spin (IS), and high spin (HS) for both Co^{3+} (LS with t_{2g}^6 and $S=0$, IS with $t_{2g}^5e_g^1$ and $S=1$, and HS with $t_{2g}^4e_g^2$ and $S=2$) and Co^{4+} (LS with t_{2g}^5 and $S=\frac{1}{2}$, IS with $t_{2g}^4e_g^1$ and $S=\frac{3}{2}$, and HS with $t_{2g}^3e_g^2$ and $S=\frac{5}{2}$). (Ref. 17)

The oxygen content of these layered cobaltites, δ , controls not only the mean valence of Co ions (which can vary from 3.5+ for $\delta=1$ to 2.5+ for $\delta=0$), but also the coordination of Co (pyramidal or octahedral) and has therefore a strong influence on the spin state of Co. This leads to the magnetic and transport properties of these compounds being mainly dominated by the oxygen content. For instance, it has been found that for low δ there is a great tendency to form charge-ordered structures and this phenomenon has been reported for YBaCo_2O_5 (Ref. 4) and $\text{TbBaCo}_2\text{O}_5$ (Ref. 5). Metal-insulator and spin-state transitions as well as successive magnetic transitions due to competing ferromagnetic-antiferromagnetic interactions are present in compounds with $\delta=0.5$ for a wide variety of rare earths.^{7-9,14,15}

In Ref. 10 we investigated the origin of this metal-insulator transition above room temperature (RT) (for $\delta=0.5$). We have attributed the changes of the electron mobility on heating to a sudden change from the Co^{3+} LS state (t_{2g}^6) to Co^{3+} HS state ($t_{2g}^4e_g^2$) in Co^{3+}O_6 octahedra.¹⁰ For $\delta=0.5$ it is well established that oxygen vacancies order forming filled and empty rows of oxygen sites along a in the RO_δ planes. Associated with this ordering, IS/LS Co^{3+} states were found to be orderly distributed in the structure below T_{MI} (IS/HS states above the spin-state transition at T_{MI}).¹⁰ This makes it such that the spin-state transition takes place in an ordered

manner (as was also suggested in Ref. 6). Moreover, giant magnetoresistance effects accompany the ferromagnetic-antiferromagnetic FM-AFM competition in $R\text{BaCo}_2\text{O}_{5.5}$ compounds. Ordering of oxygen in RO layers into alternating empty and filled rows favors a strong uniaxial anisotropy of Co^{3+} spins. In the FM phase Co spins align along the oxygen-chain direction forming ferromagnetic two-leg ladders. The interaction between them is mediated by nonmagnetic Co-O layers. Instead of FM, this coupling turns out to be weakly AFM at low temperatures.¹⁴

Little is known about the properties of the compounds with higher oxygen content. For $\delta > 0.5$ structural studies are scarce. To the best of our knowledge, besides the initial study of $\text{LaBaCo}_2\text{O}_6$ (more precisely $\text{La}_{0.5}\text{Ba}_{0.5}\text{CoO}_3$ as no order between La and Ba was reported),¹⁸ there is only a recent study, including oxygenated compounds, which suggests partial order of the oxygen vacancies into channels along a in $\text{NdBaCo}_2\text{O}_{5.69}$.¹¹

With the aim of reducing this lack of knowledge, we have prepared and characterized the structural and magnetic properties of the cobaltite $\text{PrBaCo}_2\text{O}_{5+\delta}$ with $\delta \approx 0.75$. We report the finding of a strong tendency to an order of oxygen vacancies different to that of $\delta = 0.5$ compounds. We describe the magnetic properties of this composition and confirm a different scenario (compared to $R\text{BaCo}_2\text{O}_{5.5}$ compounds) below room temperature.

II. EXPERIMENTAL

Two polycrystalline samples of $\text{PrBaCo}_2\text{O}_{5+\delta}$ cobaltite were sintered following different ways. For both specimens, the precursors were prepared by solid-state reaction in air. High-purity powders of Pr_6O_{11} , BaCO_3 , and Co_3O_4 were mixed at stoichiometric weights. After a decarbonation process (15 h at 1000°C) the mixtures were pressed into pellets, annealed at 1100°C during 24 h in air, and cooled down ($100^\circ\text{C}/\text{h}$) to RT twice. The quality of the initial compounds obtained was tested by means of laboratory x-ray diffraction. These precursors were found to be well crystallized and single phase, having the characteristic stacking sequence $[\text{CoO}_2][\text{BaO}][\text{CoO}_2][\text{LnO}_\delta]$ along the c direction.⁷ A careful study of different annealing conditions and thermal treatments was performed prior to attain the desired stoichiometry. The equilibrium value of δ as a function of oxygen pressure (p_{O_2}) and temperature was obtained by thermogravimetric analysis (TGA) within the range $250^\circ\text{C} < T < 900^\circ\text{C}$ and $10^{-5}\text{atm} < p_{\text{O}_2} < 1\text{atm}$.¹⁹ The first sample (PBC-I) was obtained by grinding the sintered bar with an agate mortar and pestle, annealing the obtained powder in pure argon at 400°C during 3 h, and cooling it slowly to room temperature. The second sample (PBC-II) was obtained by ball milling the bar with an agate grinder, annealing the powder at 250°C under low oxygen pressure of $p_{\text{O}_2} = 3.28 \times 10^{-2}\text{atm}$, and quenching it to RT. The absolute oxygen content of the quenched samples was measured by TGA reducing in dry H_2 at 1000°C and assuming Co, Pr, and BaO as final products. This rendered $\delta = 0.762(2)$ for PBC-I and $\delta = 0.74(1)$ for PBC-II.

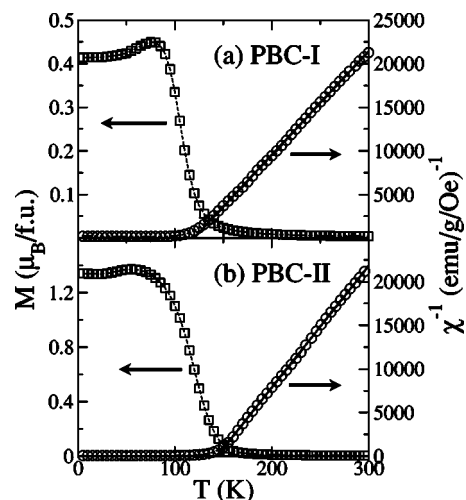


FIG. 1. Magnetization and inverse susceptibility of PBC-I (a) and PBC-II (b) samples taken under $\mu_0 H = 0.1$ T. Solid lines show the best fits of the Curie law to the inverse susceptibility.

Magnetization measurements on these two samples were performed using a superconducting quantum interferometer device (SQUID, Quantum Design) and a physical properties measuring system (PPMS, Quantum Design). Neutron powder diffraction (NPD) data were collected at the ILL (Grenoble) in the temperature range 5–300 K. Two neutron diffractometers were used: D2B ($\lambda = 1.594 \text{ \AA}$, high resolution) and D1B ($\lambda = 2.52 \text{ \AA}$). In this last diffractometer, by means of a cryomagnet, we have also performed NPD measurements up to $\mu_0 H = 4$ T. These last measurements have been done at $T = 10$ K after cooling from RT at zero field. In addition, ultrahigh-resolution synchrotron x-ray powder diffraction (SXRPD) data were collected using BM16 beamline (for PBC-I) at the European Synchrotron Radiation Facility (ESRF) in Grenoble. PBC-I sample was loaded in a borosilicate glass capillary ($\phi = 0.5$ mm) and rotated during data collection. Good-quality angle-dispersive [$\lambda = 0.450\,294(1) \text{ \AA}$] patterns were recorded at RT, the short wavelength being selected with a double-crystal $\text{Si}(1\,1\,1)$ monochromator and calibrated with Si NIST ($a = 5.430\,94 \text{ \AA}$).

III. MAGNETIZATION RESULTS

Figure 1 shows the temperature dependence of the dc magnetization and the inverse susceptibility measured under an applied field of $\mu_0 H = 0.1$ T after a field cooling process. A sudden enhancement, on cooling, of the magnetic moment, signaling a transition from a paramagnetic (PM) to a FM phase, can be well appreciated in both samples. At lower temperatures, in both cases, the $M(T)$ curve shows a maximum and a decrease (on cooling) of the magnetization, signaling perhaps some kind of antiferromagnetic ordering. From the inflection points of the $M(T)$ curves we estimate $T_C = 110(5)\text{K}$ (PBC-I) and $T_C = 120(5)\text{K}$ (PBC-II). Maxima of $M(T)$ curves are observed at $T_N = 80(5)\text{K}$ and $T_N = 65(10)\text{K}$ for PBC-I and PBC-II, respectively. This $M(T)$ evolution clearly differs from that in $R\text{BaCo}_2\text{O}_{5.5}$ com-

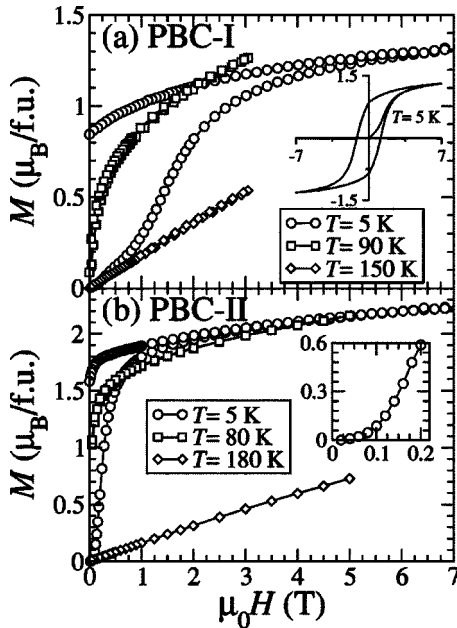


FIG. 2. (a) Isothermal magnetization curves of PBC-I at different temperatures. The inset shows the whole hysteresis cycle at $T = 5$ K. (b) The same for PBC-II sample. The insets shows an enlargement of the $M(H)$ curve at $T = 5$ K.

pounds, where a maximum around 250 K is followed by a deep and abrupt drop of the magnetization 40–60 K below the first enhancement (signaling the total disruption of the ferromagnetic ordering).

We have also recorded the isothermal magnetization curves shown in Fig. 2. $M(H)$ curves have been recorded at three temperatures: at 5 K, just above T_N , and just above T_C . These measurements have been done after a zero-field cooling from RT. It can be appreciated that, at $T = 5$ K, the first magnetization curves of PBC-I and PBC-II [see inset in Fig. 2(b)] samples present the usual instep followed by a quick rise of the magnetic moment. The field at which the quick rise starts is about 8 kOe for PBC-I and about 1 kOe for PBC-II sample. At this temperature the magnetizing process is highly irreversible as shown by the high separation between the up and down magnetization curves. This instep is absent at the other temperatures measured. Isothermal $M(H)$ curves measured just above T_N show a reversible behavior. It must also be mentioned that, contrarily to the usual behavior of a ferromagnet, the isothermal $M(H)$ curve (of PBC-I) recorded at $T = 90$ K overpasses $M(H)$ curve recorded at $T = 5$ K. This fact is not so clear for PBC-II, but, at least $M(\mu_0H = 5 \text{ T}, T = 80 \text{ K}) \approx M(\mu_0H = 5 \text{ T}, T = 5 \text{ K})$. Above T_C a standard paramagnetic behavior is recovered for both samples.

In addition to these similarities, Figs. 1 and 2 evidence some differences between the two studied samples. The first one is the different value of the low temperature magnetization (found in Fig. 1): $0.42 \mu_B/\text{f.u.}$ (PBC-I) and $1.34 \mu_B/\text{f.u.}$ (PBC-II). This difference is not only due to the fact that the applied field in the measurement (0.1 T) is above the instep in $M(H)$ curve of PBC-II but below it for PBC-I. As depicted in Fig. 2 also different magnetization

values are reached under high field ($\mu_0H = 7$ T). We have also recorded the full hysteresis cycle for both compounds [shown, for PBC-I, as an inset in Fig. 2(a)] and found differences in the remanence ($0.85 \mu_B/\text{f.u.}$ for PBC-I and $1.6 \mu_B/\text{f.u.}$ for PBC-II) and coercive field (1.15 T for PBC-I and 0.19 T for PBC-II). The differences in the magnetic behavior are reduced, but still persist, above T_C . This is reflected in the fitted Curie law to the inverse susceptibility in both compounds. These fits render $\theta_C = 125(5)$ K and $\mu_{\text{eff}} = 5.53(5) \mu_B/\text{f.u.}$ [$\mu_{\text{eff}} = 3.91(5) \mu_B/\text{Co}$] for PBC-I and $\theta_C = 145(5)$ K and $\mu_{\text{eff}} = 5.29(5) \mu_B/\text{f.u.}$ [$\mu_{\text{eff}} = 3.74(5) \mu_B/\text{Co}$] for PBC-II.

The hysteresis cycle in Fig. 2(a) (inset) is much different from the $M(H)$ curves obtained in the AFM phase of $\text{RBaCo}_2\text{O}_{5.5}$ oxides.^{9,6} In the latter, a field-induced FM moment occurs at higher critical fields and the transition has been related to the spin alignment of AF-coupled adjacent FM ladders, with Ising-like anisotropy. At variance with the behavior for $\delta = 0.5$, the low magnetization state is not recovered again by lowering the field in the case of $\delta = 0.75$ [inset of Fig. 2(a)]. Hence, the rise of magnetization observed in Fig. 2 is not reminiscent of the field-induced transition in $\text{RBaCo}_2\text{O}_{5.5}$.

IV. DIFFRACTION RESULTS

A. Order of vacancies

For PBC-I we have performed a joint Rietveld refinement of high-resolution NPD data collected at D2B and ultrahigh-resolution SXRPD data collected at BM16 (at RT). We have found that both data sets can be quite well refined using an average structure with lattice parameters $a = b \approx a_p$ and $c \approx 2a_p$ (where a_p is the perovskite cubic cell) and $P 4/mmm$ (No. 123) space group (SG). But in addition to this average structure, a set of much smaller peaks (with an intensity of about three orders of magnitude smaller than that of the most intense peak) is present. These extra peaks, which must be attributed to a particular order of oxygen vacancies in the structure, can be indexed by doubling both a and b lattice parameters (so conserving the tetragonal symmetry).

The joint refinement of these two data sets has permitted us to explore different possible ordered arrangements of the oxygen vacancies within the $[\text{PrO}_\delta]$ planes. In Fig. 3 the studied arrangements are shown. The first possibility explored [Fig. 3(a)] corresponds to a perfect order in a $2a_p \times 2a_p$ supercell in the $[\text{PrO}_\delta]$ planes, with vacancies located in $1b[(0 \ 0 \ \frac{1}{2})]$ Wyckoff position of the $P 4/mmm$ SG. The refinements confirm that this model does not reproduce well the intensity of some superstructure peaks, as can be seen in Fig. 4(a). The second model refined [Fig. 3(a)] corresponds to the location of the vacancies in $(1 \ 0 \ 0)$ lines, in a similar manner to the order in $\delta = 0.5$ layered cobaltites. In the present case, due to the smaller concentration of vacancies, these lines would be partially occupied forming a solid solution with oxygen ions. Using this model, the refinement leads to a very poor agreement with the experimental intensities. As can be seen in Fig. 4(b) the agreement is clearly worse than that obtained with the first model. To be men-

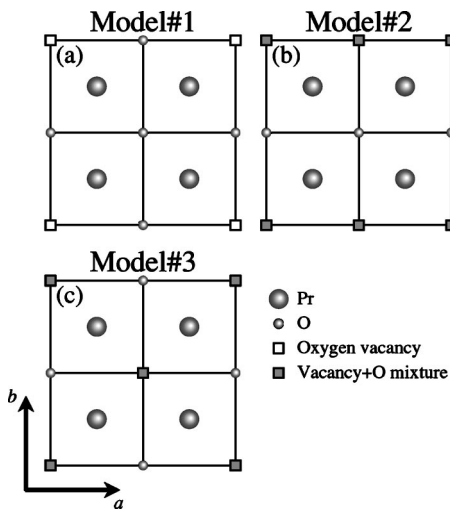


FIG. 3. Schematic picture of the $z=0.5$ mirror plane showing the different ordered arrangements of vacancies adjusted. (a) Complete order in a 2×2 structure. (b) Solid solution of the order found in $\delta=0.5$ layered cobaltites. (c) Solid solution in alternating $(1\ 1\ 0)$ lines.

tioned is that this second model violates the fourfold symmetry of the tetragonal $P\ 4/mmm$ SG and, consequently, we used the $P\ mmm$ (No. 47) SG, with the constraint $b=2a$. The third possibility corresponds to an imperfect order of the $2a_p \times 2a_p$ structure, in which vacancies are inhomogeneously distributed between $1b[(0\ 0\ \frac{1}{2})]$ and $1d[(\frac{1}{2}\ \frac{1}{2}\ \frac{1}{2})]$ Wyckoff positions of the $P\ 4/mmm$ SG. This last model for the order of oxygen vacancies provides the best agreement with the experimental intensities. The first model tried corresponded to the particular case of having an occupation 0 and 100% of $1d$

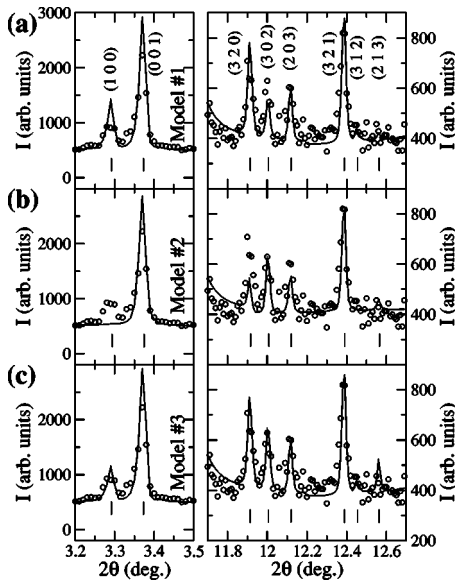


FIG. 4. Portions of the SXRPD refinements of PBC-I sample at RT showing some of the peaks attributed to the ordering of vacancies. Rows labeled (a), (b), and (c) correspond to model Nos. 1, 2, and 3 in Fig. 3, respectively. It must be noted that the most intense peak of the diffraction pattern is about 3.5×10^5 units, three orders of magnitude larger than peaks coming from vacancy order.

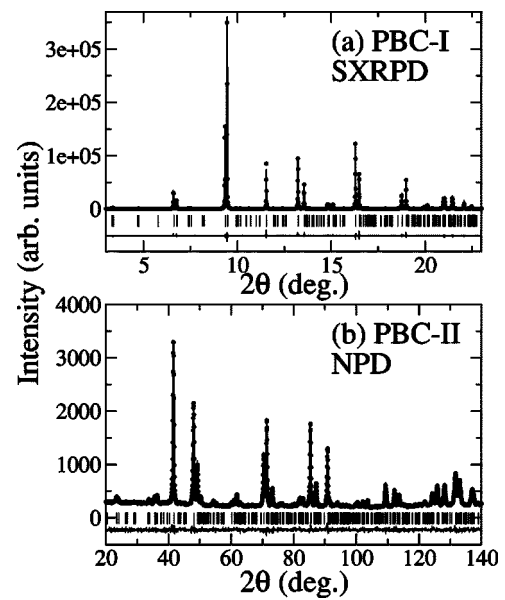


FIG. 5. Adjusted patterns following model No. 3 in Fig. 3 of (a) SXRPD data from the PBC-I sample and (b) NPD data from the PBC-II sample.

and $1b$ positions, respectively. In PBC-I the refinement converges to the 25% of vacancies located in the $1d$ position and the remaining 75% in the $1b$ position. It is apparent that with this relaxation of the perfect $2a_p \times 2a_p$ order, the experimental intensities shown in Fig. 4(c) are now much better reproduced. The whole refinement, according to the last model, of SXRPD data is shown in Fig. 5(a).

It is worth mentioning that, in addition to superstructure peaks doubling a and b lattice parameters (from a_p), a single peak, with similar intensity and shape to those shown in Fig. 4, is clearly visible in SXRPD pattern (of PBC-I sample). This peak can only be indexed by doubling c lattice parameter.

Analysis of the superstructure reflections and vacancy order was extended to the second sample. We successfully refined the high-resolution NPD data of PBC-II using the same model, as is shown in Fig. 5(b). The refinement rendered a smaller degree of order between vacancies and oxygen atoms: 35% of vacancies in $1d$ and 65% in $1b$ Wyckoff positions.

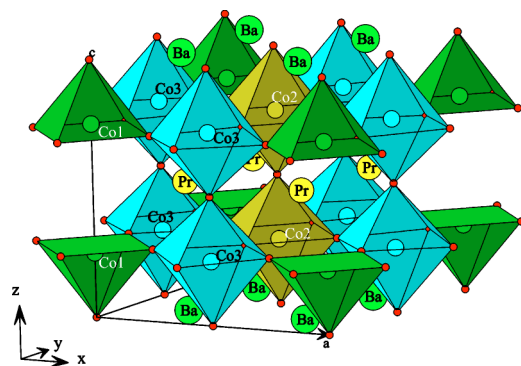


FIG. 6. (Color online) Polyhedral view of the idealized order (model No. 1). Cations within the unit cell are labeled accordingly to notation used in Table I.

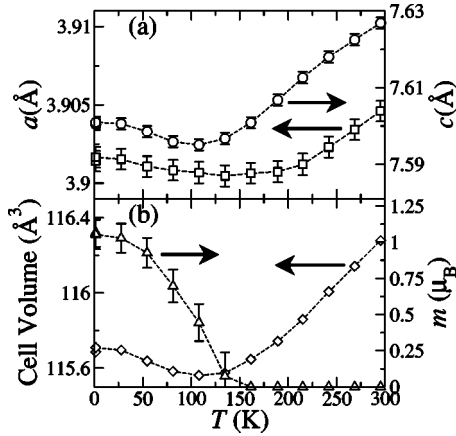


FIG. 7. (a) Cell parameters, as a function of temperature obtained for PBC-I (open symbols) and PBC-II (solid symbols), using low-resolution and high-resolution NPD, respectively. a (left axis) corresponds to squares and c (right axis) corresponds to circles. (b) Cell volume (\diamond , left axis) and ordered magnetic moment (Δ , right axis) found by low-resolution NPD data.

According to our findings about the order of oxygen vacancies, a schematic view of the structure of $\text{PrBaCo}_2\text{O}_{5.75}$ is shown in Fig. 6. For sake of simplicity we have represented the perfect order of the $2a_p \times 2a_p$ structure with 0% of vacancies (100% of oxygen) in $1d(\frac{1}{2}\frac{1}{2}\frac{1}{2})$ sites and 100% of vacancies (0% of oxygen) in the $1b(0\ 0\ \frac{1}{2})$ position.

B. Structural study and thermal evolution

A temperature-dependent neutron diffraction study was carried out on a PBC-I sample on the medium-resolution D1B diffractometer of the Institute Laue-Langevin in Grenoble in the temperature range 1.5–300 K. D1B is optimized for monitoring cell variations and the magnetic contribution. These patterns are not suitable for precise structure refinement and have been analyzed using the average $P\ 4/mmm$ SG with $a \approx a_p$ and $c \approx 2a_p$. At low temperature the apparition of AFM ordering is evidenced by the appearance of reflections that enlarge this structural cell. The details of the magnetic structure are discussed in the next subsection. The lattice parameters found, as a function of temperature, are depicted in Fig. 7(a) (open symbols). To be emphasized is that, on cooling, the thermal contraction stops at $T_N=135$ K and, instead, a low-temperature expansion takes place in both a and c parameters. This gives rise to a cell volume expansion on cooling that has been depicted in Fig. 7(b).

For PBC-II sample, high-resolution NPD data (D2B) were collected at $T=10$ K, 175 K, and RT. The structural details obtained from Rietveld refinements of these data are listed in Table I. The occupancies of $1b$ [O(2a)] and $1d$ [O(2b)] Wyckoff positions have been refined constraining the total oxygen content to the experimental value $\delta=0.74$. We have checked that relaxing this constraint does not improve the refinement appreciably and that the obtained value of δ is, within the errors, the same. Refinements at the three temperatures converged to very similar distribution of vacancies.

TABLE I. Structural details and agreement factors found from high-resolution powder diffraction at different temperatures. At all the temperatures the refinements have been done using the $P4/mmm$ SG. Wyckoff positions of the different ions are $4j$, $(x\ x\ 0)$, for Ba; $4k$, $(x\ x\ \frac{1}{2})$, for Pr; $2g$, $(0\ 0\ z)$, for Co(1); $2h$, $(\frac{1}{2}, \frac{1}{2}, z)$, for Co(2); $4i$, $(0, \frac{1}{2}, z)$, for Co(3); $1a$, $(0\ 0\ 0)$, for O(1a); $1c$, $(\frac{1}{2}, \frac{1}{2}, 0)$, for O(1b); $2f$, $(0, \frac{1}{2}, 0)$, for O(1c); $1b$, $(0\ 0\ \frac{1}{2})$, for O(2a); $1d$, $(\frac{1}{2}, \frac{1}{2}, \frac{1}{2})$, for O(2b); $2e$, $(0, \frac{1}{2}, \frac{1}{2})$, for O(2c); $8s$, $(x, 0, z)$, for O(3a); and $8t$, $(x, \frac{1}{2}, z)$, for O(3b). O(2a) and O(2b) are just partially occupied. The occupancy factors found are reported in the table.

		PBC-II	PBC-I	PBC-I
		10 K	175 K	300 K
$a(\text{\AA})$		7.7954(1)	7.8007(1)	7.8218(1)
$c(\text{\AA})$		7.5941(1)	7.6057(1)	7.6353(1)
$V(\text{\AA}^3)$		461.47(1)	462.82(1)	467.13(1)
Ba	x	0.2503(7)	0.2499(8)	0.2500(7)
Pr	x	0.2535(9)	0.2543(8)	0.2575(7)
Co(1)	z	0.250(2)	0.254(2)	0.249(2)
Co(2)	z	0.244(2)	0.246(2)	0.247(2)
Co(3)	z	0.254(2)	0.254(2)	0.251(2)
O(2a)occup.		0.33(3)	0.32(3)	0.35(3)
O(2b)occup.		0.65(3)	0.66(4)	0.63(3)
O(3a)	x	0.2468(9)	0.2460(8)	0.2437(7)
	z	0.2888(3)	0.2871(3)	0.2875(3)
O(3b)	x	0.2501(8)	0.2488(7)	0.2495(7)
	z	0.2693(3)	0.2705(2)	0.2702(3)
χ^2		4.5	3.6	2.9
R_B		3.4	3.3	2.9

^aSXRPD pattern.

^bNPD pattern.

In the structure summarized in Table I there are three different crystallographic positions occupied by Co. Co(3) in $4i$ only presents octahedral coordination (100% in octahedra). For Co(1) in $2g$, dominant coordination is pyramidal (77% for PBC-I and 65% for PBC-II, respectively). Inversely, the majority of Co(2) in $2h$ presents octahedral coordination (29% for PBC-I and 34% for PBC-II).

Table II lists Co-O bond distances found for these three Co sites as well as the basal Co-O-Co bond angles. (All apical Co-O-Co bond angles are 180° by symmetry restrictions.) Concerning the Co-O distances, the evolution depends on the Co site. In the paramagnetic region a contraction of $\langle d_{\text{Co}(3)\text{-O}} \rangle$ by about $\sim 1.5 \times 10^{-2}$ \AA is observed on cooling between 300 and 175 K. This evolution is opposite to that of the mean Co(1)-O bond length, which displays a tiny expansion in the same interval. On cooling from 175 to 10 K, the small expansion of $\langle d_{\text{Co}(1)\text{-O}} \rangle$ contrasts with the tiny shrinking of $\langle d_{\text{Co}(2)\text{-O}} \rangle$ and $\langle d_{\text{Co}(3)\text{-O}} \rangle$ bonds.

C. Magnetic order

Qualitatively, we have observed very similar behavior of magnetic intensities in the NPD patterns of both samples. On

TABLE II. Co-O bond distances (in Å) and Co-O-Co bond angles obtained from details reported in Table I. O(3a) and O(3b) are basal oxygens while O(1*i*) and O(2*i*) (with $i=a, b$, and c) are apical ones.

	10 K	PBC-II 175 K	300 K	PBC-I 300 K
$d_{\text{Co}(1)\text{-O}(1a)}$ (Å)	1.90(1)	1.93(1)	1.90(1)	1.907(8)
$d_{\text{Co}(1)\text{-O}(2a)}$ (Å) ^a	1.90(1)	1.87(1)	1.92(1)	1.908(8)
$d_{\text{Co}(1)\text{-O}(3a)}$ (Å)($\times 4$)	1.947(7)	1.936(7)	1.929(6)	1.94(1)
$d_{\text{Co}(2)\text{-O}(1b)}$ (Å)	1.86(1)	1.87(1)	1.89(1)	1.921(8)
$d_{\text{Co}(2)\text{-O}(2b)}$ (Å) ^b	1.94(1)	1.93(1)	1.93(1)	1.894(8)
$d_{\text{Co}(2)\text{-O}(3b)}$ (Å)($\times 4$)	1.958(6)	1.968(7)	1.967(6)	1.98(1)
$d_{\text{Co}(3)\text{-O}(1c)}$ (Å)	1.93(1)	1.93(1)	1.92(1)	1.903(6)
$d_{\text{Co}(3)\text{-O}(2c)}$ (Å)	1.87(1)	1.87(1)	1.89(1)	1.912(6)
$d_{\text{Co}(3)\text{-O}(3a)}$ (Å)($\times 2$)	1.991(7)	1.998(7)	2.023(6)	2.01(1)
$d_{\text{Co}(3)\text{-O}(3b)}$ (Å)($\times 2$)	1.953(1)	1.945(1)	1.957(1)	1.939(1)
$\langle d_{\text{Co}(1)\text{-O}} \rangle$ (Å)	1.934(4)	1.930(4)	1.923(3)	1.933(2)
$\langle d_{\text{Co}(2)\text{-O}} \rangle$ (Å)	1.938(4)	1.947(4)	1.949(3)	1.961(2)
$\langle d_{\text{Co}(3)\text{-O}} \rangle$ (Å)	1.947(3)	1.948(3)	1.963(3)	1.951(2)
$\theta_{\text{Co}(1)\text{-O}(3a)\text{-Co}(3)}$ (deg)	163.6(3)	165.2(3)	163.4(3)	163.5(6)
$\theta_{\text{Co}(2)\text{-O}(3b)\text{-Co}(3)}$ (deg)	171.0(3)	170.7(2)	170.7(2)	171.0(6)

^aPartially formed [29(2)% for PBC-I and 32(3)% for PBC-II].

^bPartially formed [65(4)% for PBC-I and 77(2)% for PBC-II].

cooling across T_N , the appearance of the (1 1 1) reflection (referred to the $2a_p \times 2a_p \times 2a_p$ cell) confirms the onset of long-range AFM order. This peak signals the presence of G -type AFM order in the system, which was confirmed by our magnetic refinements. This AFM order does not require an expanded magnetic cell. In addition, other intensity changes confirm the development of ferromagnetic order. In particular, there is an enhancement of preexisting (2 0 0), and (0 0 2) peaks that can only be attributed to FM order (see Fig. 8). Taking these considerations into account, the best refinements of low-temperature NDP data corresponding to PBC-I (collected using D1B at 1.5 K) and PBC-II (collected

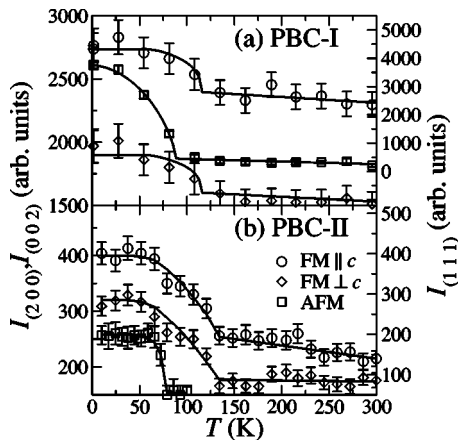


FIG. 8. Integrated intensity of (left axis) (2 0 0) (○) and (0 0 2) (□) and (right axis) (1 1 1) (◇) peaks corresponding to (a) PBC-I and (b) PBC-II samples. Solid lines are guides to the eye.

using D2B at 10 K) samples have been obtained by assuming a canted G -type AFM structure ($R_{\text{mag}}=7.3\%$ and 6.7% for PBC-I and PBC-II, respectively). In both samples, the AFM moments (μ_{AFM}) are aligned along the $(1\bar{1}0)$ direction. On the other hand, the ferromagnetic moments (μ_{FM}) are taken to be perpendicular to this direction and are composed of an in-plane [along (1 1 0)] component and an out-of-plane (along c) component. For PBC-I the refinement renders an AFM component $\mu_{\text{AFM}}=0.9(1)\mu_{\text{B}}$ and a FM one $\mu_{\text{FM}}=0.8(1)\mu_{\text{B}}$ [$m_T=1.2(1)\mu_{\text{B}}$]. For PBC-II sample, it renders $\mu_{\text{AFM}}=0.3(1)\mu_{\text{B}}$ and $\mu_{\text{FM}}=1.3(1)\mu_{\text{B}}$ [$m_T=1.3(1)\mu_{\text{B}}$]. The magnetic structures obtained for each sample are detailed in Table III. In both cases magnetic refinements have been done assuming identical magnetic moments for all Co ions [Co(1), Co(2), and Co(3) sites]. Although the spin state of Co ions, and thus their magnetic moment, can be strongly influenced by their coordination,¹⁷ the number of magnetic peaks in powder patterns does not allow to refine, with confidence, different magnetic moments in relation to the three distinguishable crystallographic positions of Co.

Figure 8 shows the temperature dependence of the integrated intensity of the three most characteristic magnetic peaks. In accordance with the thermal evolution of magnetization depicted in Fig. 1, we have found, on cooling, first an enhancement of FM (2 0 0)-(0 0 2) and, afterward, the appearance of AFM (1 1 1) peaks. The evolution shown in Fig. 8 permits us to estimate the Curie and Néel temperatures of both samples: $T_C=115(10)\text{K}$, $T_N=80(10)\text{K}$ for PBC-I and $T_C=135(10)\text{K}$, $T_N=70(10)\text{K}$ for PBC-II. These values are fairly comparable with those obtained from magnetic measurements.

Finally, we have investigated the possibility that the enhancement of $M(H)$ curves at 5 K, shown in Fig. 2, corresponds to the disruption of the AFM structure due to the field as has been reported to happen (at larger fields) for $\text{RBaCo}_2\text{O}_{5.5}$ compounds. For this we have collected NPD data at 10 K under a magnetic field, after a zero-field cooling process, up to 4 T for PBC-II sample. Figure 9(a) shows the measured intensity near $2\theta=32^\circ$ corresponding to (1 1 1) reflection. To compare, Fig. 9 shows the same region but presenting data corresponding, at zero field, to 10 and 100 K where the disappearance of this peak above T_N can be clearly appreciated. Figure 9(c) shows that the integrated intensity of (1 1 1) magnetic reflection is not affected by the field between 0 and 4 T. The same can be said for the (2 0 0) and (0 0 2) reflections.

V. DISCUSSION AND CONCLUSIONS

According to joint NPD and SXRPD refinements, for $\text{PrBaCo}_2\text{O}_{5.75}$ the location of oxygen vacancies in $\text{PrO}_{0.75}$ planes does not correspond the ordering into channels as reported for $\text{RBaCo}_2\text{O}_{5.5}$ compounds. For $\text{PrBaCo}_2\text{O}_{5.75}$ we have observed an imperfect order of these vacancies consisting in the preferential occupation of the 1*b* position. Partial disorder is restricted to a solution with atoms in 1*b* and 1*d* Wyckoff positions of the $P4/mmm$ SG. The concentration of oxygen ions in these positions confirms the same prefer-

TABLE III. Detailed magnetic structure found for PBC-I and PBC-II samples at low temperature.

Co position ^a	PBC-I			PBC-II		
	$m_x(\mu_B)$	$m_y(\mu_B)$	$m_z(\mu_B)$	$m_x(\mu_B)$	$m_y(\mu_B)$	$m_z(\mu_B)$
$(0\ 0\ z_1) - (\frac{1}{2}\ \frac{1}{2}\ z_2)$	-0.14(7)	1.13(8)	0.35(8)	0.65(6)	1.06(7)	0.49(7)
$(\frac{1}{2}\ 0 - z_3) - (0\ \frac{1}{2} - z_3)$						
$(0\ 0 - z_1) - (\frac{1}{2}\ \frac{1}{2} - z_2)$	1.13(8)	-0.14(7)	0.35(8)	1.06(7)	0.65(6)	0.49(7)
$(\frac{1}{2}\ 0\ z_3) - (0\ \frac{1}{2}\ z_3)$						
	μ_{AFM}	$\mu_{FM}^{(1\ 1\ 0)}$	$\mu_{FM}^{(0\ 0\ 1)}$	μ_{AFM}	$\mu_{FM}^{(1\ 1\ 0)}$	$\mu_{FM}^{(0\ 0\ 1)}$
	0.9(1)	0.7(1)	0.35(8)	0.3(1)	1.2(1)	0.49(7)

^a z_1 , z_2 , and z_3 stand for z of Co(1), Co(2), and Co(3), respectively. The corresponding values are those listed in Table I.

ential ordering in samples PBC-I and PBC-II (being 75%–25% and 65%–35%, respectively). In order to get samples with a perfect ordering (with all vacancies in 1*d* Wyckoff position) it is important to emphasize that the main difference in heat treatments between the two samples is that PBC-I was slowly cooled from 400°C while PBC-II was quenched from 250°C. Hence, apparently, it is below this last temperature where the oxygen order can be improved. It is of interest to recall that an order-disorder transition of oxygen vacancies in YBaCo₂O_{5.5} has been described at about 230°C (Ref. 20).

In spite of the great similarities in the magnetic behavior between the two studied compounds, we have found a certain number of differences: the value of the FM and AFM components at low temperature (which is also reflected on the remanent magnetization), the behavior of the first magnetization curve, the coercive fields, and small differences in Néel and Curie temperatures. These discrepancies may be related to two dissimilarities between the samples: the oxygen content and the degree of vacancy ordering. The variation in the oxygen content is very small, and we discard it as the origin of these differences. In contrast, we argue that the

difference in the degree of vacancy ordering can be of significance. This order must govern the magnetic interactions, and a decrease of the degree of order drives a decrease of the AFM strength, leading to a decrease of the Néel temperature and AFM ordered moment at low T , as found. This degree of order can also influence the magnetic anisotropy and thus change the first magnetization behavior and also the coercive field. It cannot be discarded that a perfect ordering of vacancies will drive a total disappearance of FM order, leading to a pure AFM arrangement of moments at low temperature, as happens in $\delta=0.5$.

From magnetic NPD data we can conclude that the low-temperature magnetic order consists of a canted AFM G -type structure. Interestingly, AFM and FM orders do not develop simultaneously. The onset of both kind of magnetic ordering is separated by about 40–50 K, the FM coupling appearing first. Temperature and field-dependent measurements shown in Figs. 1, 2, and 8 strongly suggest that a scenario of phase-separated FM and AFM zones has to be ruled out. For this conclusion it is clearer to discuss the results of PBC-I sample showing similar AFM and FM contributions ($\mu_{AFM} \approx 0.9\ \mu_B$ vs $\mu_{FM} \approx 0.8\ \mu_B$). First, a decrease of the magnetization is observed at T_N . Second, Fig. 2(a) confirms that, for the same applied field (sweep-up process), the magnetization at 90 K (between T_N and T_C) is higher than the magnetization at 5 K (below T_N), even though thermal fluctuations are more important (at 90 K). Third, from the temperature evolution of magnetic intensities (NPD) in Fig. 8, an apparent slowdown in the development of FM moment can be observed coinciding with the onset of AFM order. Therefore, the most probably scenario corresponds to FM and AFM order being interpenetrated, defining a proper canted magnetic structure. Another interesting feature is the evolution across T_N of the FM macroscopic magnetization at very low field. In Fig. 2(a) at 90 K (between T_N and T_C) we observe a FM low-field signal. In contrast, at 5 K (below T_N), this low-field signal vanishes in the isothermal measurement. It should also be noted that the field necessary for the rise of magnetization increases with the proportion of AFM component. This reinforces the interrelation between the AFM and FM ordering.

The evolution of the G -type AFM signal under field, depicted in Fig. 9(a) confirms that the rise of magnetization at $\mu_0 H = 0.1$ T in Fig. 2(b) [and presumably in Fig. 2(a) at $\mu_0 H = 0.8$ T] is not related to the disruption of the AFM or-

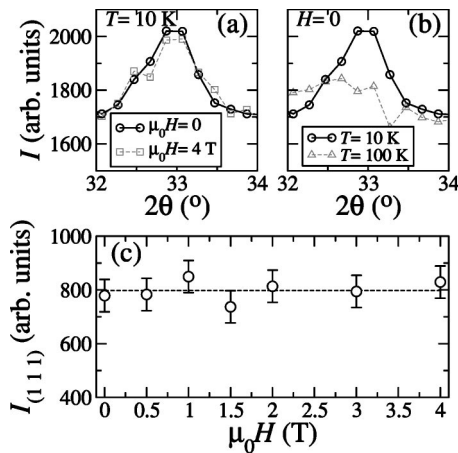


FIG. 9. Results of the NPD under a magnetic field. Panel (a) shows the measured intensity corresponding to the (1 1 1) AFM peak at 0 and 4 T and $T=10$ K. For comparison panel (b) shows the same peak at zero field, at $T=10$ and 100 K (above T_N). Panel (c) shows the evolution of the integrated intensity of the (1 1 1) AFM peak with field.

der. No changes on the integrated intensity of (1 1 1) peak can be appreciated between $\mu_0 H=0$ and 4 T. This result, together with the fact that no anomaly in M - H curves appear above 4 T, tells us that the magnetization values obtained at $\mu_0 H=7$ T (Fig. 2) do not correspond to fully polarized moments. Indeed, the total moment found by refinement of NPD data is larger than that found by magnetization measurements, but the FM component from both techniques is very consistent. From the extrapolation of high-field magnetization to zero we obtain $\mu_{FM}=0.6(1)\mu_B/\text{Co}$ for PBC-I and $\mu_{FM}=0.9(1)\mu_B/\text{Co}$ for PBC-II [to be compared with $\mu_{FM}=0.8(1)\mu_B/\text{Co}$ for PBC-I and $\mu_{FM}=1.3(1)\mu_B/\text{Co}$ for PBC-II from NPD data]. In both samples the ordered magnetic moment at low temperature is similar, $m_T=(1.2-1.3)\mu_B/\text{Co}$.

This total ordered moment from neutrons must be compared with the effective paramagnetic moment found above T_C . A very appealing result of this study is the large value of the paramagnetic moment found above T_C : $\mu_{\text{eff}}\approx 3.8\mu_B/\text{Co}$ [respectively, 3.91(5) and 3.74(5) μ_B/Co for PBC-I and PBC-II]. This value is considerably larger than the value found below T_{MI} for $\text{RBaCo}_2\text{O}_{5.5}$ ($\mu_{\text{eff}}\approx 1.8\mu_B/\text{Co}$). Immediately, the question of whether the spin transition has been shifted to much lower temperatures (well below RT) or even suppressed in the present case naturally arises. Assuming that the angular moment of Co ions is quenched ($g=2$), this result leads us to a significant conclusion: μ_{eff} in the paramagnetic phase (below 300 K) is not compatible with the presence of Co^{3+} ions in low spin. Effectively, according to oxygen content, Co^{3+} and Co^{4+} coexist at a ratio 3:1. Taking into account the three spin states of both Co^{3+} and Co^{4+} and the presence of two types of coordinations (pyramids and octahedra) several possibilities arise, but different facts must be taken into account. First, a larger Co valence (Co^{4+}) prefers a larger coordination (octahedral). Second, pyramidal Co^{3+} strongly tends to present IS.¹⁷ With these considerations 50% of Co will correspond to Co^{3+} in octahedra. Let us suppose that, as happens in $\text{RBaCo}_2\text{O}_{5.5}$, these are in LS. If the other Co^{3+} are assumed to be in pyramids (presumably, in IS state) and Co^{4+} in octahedra the effective paramagnetic moment will be $\mu_{\text{eff}}=1.66\mu_B/\text{Co}$ (Co^{4+} in LS), $\mu_{\text{eff}}=2.40\mu_B/\text{Co}$ (Co^{4+} in IS), or $\mu_{\text{eff}}=3.28\mu_B/\text{Co}$ (Co^{4+} in HS), all being below the obtained value. On the other hand, if Co^{3+} in octahedral coordination would be in HS, Co^{3+} in pyramids in IS, and Co^{4+} in LS, the effective magnetic moment expected would be $\mu_{\text{eff}}=3.84\mu_B/\text{Co}$, fairly comparable with the experimental value.

From this picture one would expect an average magnetic moment for neutrons of $\mu_T\approx 2.75\mu_B/\text{Co}$ and therefore more than twice the observed ordered moment [(1.2–1.3) μ_B/Co] at low temperature. At this point two possibilities should be discussed. One possible explanation could be the presence of magnetic disorder due to imperfect oxygen ordering leading to frustration. A second possibility is the occurrence of changes in the spin configuration of some Co ions between T_C and the lowest temperature. Regarding the first possibility, it must be mentioned that the same value of m_T is found even when PBC-I is less disordered than PBC-II. Regarding the second possibility, we have not detected any feature in

the lattice evolution of the structure that could be indicative of spin state changes between low temperature and the deviation from the Curie-Weiss law (at T_C). As explained in the precedent section, there is a lattice anomaly within the aforementioned temperature interval: an elongation of the c axis and volume expansion below T_N . However, a cell contraction is expected if a change to a low-spin state takes place on cooling. Nevertheless, the magnitude this contraction (on cell volume and cell parameters) reported for $\text{RBaCo}_2\text{O}_{5.5}$ is considerably smaller than the changes shown near T_N in Fig. 7. Thus, the cell anomaly due to a spin-state transition could be hidden by the changes due to the magnetoelastic coupling. A definitive answer to this point cannot be inferred from present results and further investigations will be necessary.

The absence of LS Co^{3+} ions below RT implies a different scenario accepted for samples with $\delta=0.5$. For them, half of Co sites (octahedra) were reported to be in Co^{3+} LS below the spin-state transition around 360 K. At this point, it is interesting to highlight the fact that $\text{PrBaCo}_2\text{O}_{5+\delta}$ with $\delta=0.7(1)$ in Ref. 7 is metallic well below RT. This will be in accordance with the presence of Co^{3+} in HS, as in $\delta=0.5$ compounds where the metallic state is induced by the spin state transition to HS of Co^{3+} ions.

VI. SUMMARY

To summarize, we have prepared and characterized, by different techniques, two samples of $\text{PrBaCo}_2\text{O}_{5+\delta}$ with $\delta\approx 0.75$. By means of NPD and SXRPD data we have found that the most likely distribution of oxygen vacancies in the $\text{PrO}_{0.75}$ planes corresponds to an imperfect order in which vacancies are inhomogeneously distributed along the diagonals of these planes. The structure, with this order, is found to be tetragonal ($P4/mmm$ SG) with $a\approx c\approx 2a_p$. This order contrasts with the location, along (0 1 0) lines found in $\delta=0.5$ compounds, driving to orthorhombic structures.^{8,10}

Magnetization and NPD data show that, on cooling, both samples present a paramagnetic-to-FM transition. Afterward, there is a FM-to-AFM transition. These two transitions are also found in $\delta=0.5$ compounds but at considerably higher temperatures.⁷ We have found that the FM-to-AFM transition is not complete. Thus, a certain FM moment persists below T_N . Results presented exclude the possibility of a phase-separated scenario and a true canted AFM structure is concluded. The low-temperature FM moment is different in both samples. We attribute this difference to the different degree of order in the studied samples, and the possibility of an exclusive AFM ordering for a perfect order of vacancies is suggested. We report a considerable volume expansion (on cooling) concomitant with the appearance of magnetic order. We also show that the low-temperature magnetic structure is stable up to $\mu_0 H=7$ T.

Above T_C (and below RT) the effective paramagnetic moment of Co ions is considerably large. This strongly indicates that Co^{3+} ions in an octahedral environment are not in the LS (as in $\delta=0.5$ compounds below RT),¹⁰ but in the HS state. This is consistent with the low values of the resistivity found in this compound for similar values of δ (Ref. 7).

ACKNOWLEDGMENTS

Financial support by the CICYT (Grant No. MAT2003-07483-C02-02) and Generalitat de Catalunya (Grant Nos. GRQ95-8029, PICS2003-15) is thanked. C.F. acknowledges

financial support from MCyT (Spain) and fruitful discussions with Dr. Ll. Balcells. We thank ILL and ESRF for the provision of neutron and synchrotron beam time. We thank E. Suard (ILL) and E. Doryee (ESRF) for help during data collection.

-
- ¹A. Maignan, L. B. Wang, S. Hébert, D. Pelloquin, and B. Raveau, *Chem. Mater.* **14**, 1231 (2002).
- ²M. Hervieu, A. Maignan, C. Michel, V. Hardy, N. Créon, and B. Raveau, *Phys. Rev. B* **67**, 045112 (2003).
- ³S. Tsubouchi, T. Kyōmen, M. Itoh, P. Ganguly, M. Oguni, Y. Shimojo, Y. Morii, and Y. Ishii, *Phys. Rev. B* **66**, 052418 (2002).
- ⁴T. Vogt, P. M. Woodward, P. Karen, B. A. Hunter, P. Henning, and A. R. Moodenbaugh, *Phys. Rev. Lett.* **84**, 2969 (2000).
- ⁵E. Suard, F. Fauth, V. Caignaert, I. Mirebeau, and G. Baldinozzi, *Phys. Rev. B* **61**, R11 871 (2000).
- ⁶I. O. Troyanchuk, N. V. Kasper, D. D. Khalyavin, H. Szymczak, R. Szymczak, and M. Baran, *Phys. Rev. Lett.* **80**, 3380 (1998).
- ⁷A. Maignan, C. Martin, D. Pelloquin, N. Nguyen, and B. Raveau, *J. Solid State Chem.* **142**, 247 (1999).
- ⁸Y. Moritomo, T. Akimoto, M. Takeo, A. Machida, E. Nishibori, M. Takata, M. Sakata, K. Ohoyama, and A. Nakamura, *Phys. Rev. B* **61**, R13 325 (2000).
- ⁹M. Respaud, C. Frontera, J. L. García-Muñoz, M. A. G. Aranda, B. Raquet, and J. M. Broto, *Phys. Rev. B* **64**, 214401 (2001).
- ¹⁰C. Frontera, J. L. García-Muñoz, A. Llobet, and M. A. G. Aranda, *Phys. Rev. B* **65**, 180405 (2002).
- ¹¹J. C. Burley, J. F. Mitchell, S. Short, D. Miller, and Y. Tang, *J. Solid State Chem.* **170**, 339 (2003).
- ¹²A. A. Taskin, A. N. Lavrov, and Y. Ando, *Proceedings of the 22nd International Conference on Thermoelectrics, La Grande-Motte, France (IEEE, 2003)*, pp. 196–199.
- ¹³F. Fauth, E. Suard, V. Caignaert, and I. Mirebeau, *Phys. Rev. B* **66**, 184421 (2002).
- ¹⁴A. A. Taskin, A. N. Lavrov, and Y. Ando, *Phys. Rev. Lett.* **90**, 227201 (2003).
- ¹⁵D. D. Khalyavin, S. N. Barilo, S. V. Shiryayev, G. L. Bynchkov, I. O. Troyanchuk, A. Furrer, A. Allenspach, H. Szymczak, and R. Szymczak, *Phys. Rev. B* **67**, 214421 (2003).
- ¹⁶M. A. Señaris-Rodríguez and J. B. Goodenough, *J. Solid State Chem.* **116**, 224 (1995).
- ¹⁷M. Pouchard, A. Nillesuzanne, and J. P. Doumerc, *J. Solid State Chem.* **162**, 282 (2001).
- ¹⁸E. Suard, F. Fauth, and V. Caignaert, *Physica B* **276**, 254 (2000).
- ¹⁹A. Caneiro, P. Bavdaz, J. Fouletier, and J. P. Abriata, *Rev. Sci. Instrum.* **53**, 1072 (1982).
- ²⁰D. Akahoshi and Y. Ueda, *J. Phys. Soc. Jpn.* **68**, 736 (1999).